Hyperspectral imagery to discriminate weeds in wheat

Gilles Rabatel, F. Ougache, N. Gorretta, M. Ecarnot

Hyperspectral imagery to discriminate weeds in wheat

G. Rabatel*. F. Ougache**

N. Gorretta*, M. Ecarnot***

**UMR ITAP – Cemagref Montpellier*
361, rue J-F Breton, BP 5095 – 34196 Montpellier Cedex 5, France

(e-mail: gilles.rabatel@ cemagref.fr)

***Université Montpellier II, place Eugène Bataillon*

34095 Montpellier cedex 5, France

****UMR AGAP - INRA Montpellier*
2 PLACE VIALA, 34060 Montpellier cedex 1, France

Abstract: The problem of weed and crop discrimination by computer vision remains today a major obstacle to the promotion of localized weeding practices. The objective of present study was to evaluate the potential of hyperspectral imagery for the detection of dicotyledonous weeds in durum wheat during weeding period (end of winter). An acquisition device based on a push-broom camera mounted on a motorized rail has been used to acquire top-view images of crop at a distance of one meter. A reference surface set in each image, as well as specific spectral preprocessing, allow overcoming variable outdoor lighting conditions. The spectral discrimination between weeds and crop, obtained by PLS-DA, appears particularly efficient, with a maximal error rate on pixel classification lower than 2%. However complementary studies addressing robustness are still required.

1. Introduction

The Precision Agriculture concept relies on the spatial modulation of crop processing operations, for a better adaptation to heterogeneities inside the parcel. This concept, which raised more than twenty years ago, is now currently applied in nitrogen input management, allowing a better control on yield and product saving.

However, for weeding operations, despite considerable environmental and economical issues, the common practice until now is still to apply an assurance strategy: herbicides are uniformly spread all over the parcel whatever is the actual level of infestation.

The reason is mainly technological. Actually some devices are proposed on the market to operate localized spraying of herbicides on bare soil (the vegetation being detected by photocells). However, no commercial setup addresses localized weeding operations after crop emergence, because it requires a perception system based on computer vision, able to discriminate weeds from crop.

Indeed, the identification of species inside vegetation is today the main obstacle to localized weeding. Numerous scientific studies have addressed this problem, and can be classified in two main approaches (Slaughter, D et al. 2008):

- the spectral approach, which focuses on the plant reflectance, and involves multispectral or hyperspectral imagery (Feyaerts and van Gool, 2001) (Vrindts et al. 2002). In this case, the difficulty consists in establishing spectral differences that are robust with respect to variable lighting conditions.

- the spatial approach, which relies on spatial criteria such as plant morphology (Chi, Y et al. 2003, Manh et al. 2001), texture (Burks, T et al. 2000) or spatial organization (Gée et al, 2008). In this case, the natural complexity and variability of vegetation scenes are the main difficulties.

The study presented here comes within the first approach, in the particular case of durum wheat crop. The objective was to evaluate, as a first step, if the leaf reflectance contains enough spectral information to make a reliable discrimination between crop and dicotyledonous weeds. For this purpose, hyperspectral images of crop scenes have been acquired during the weeding period. Then specific correction procedures have been applied to overcome the variability of lighting conditions and of spatial orientation of leaves in natural crop scenes. Finally, a PLS-DA discrimination model has been calibrated and tested on the resulting hyperspectral images, and the discrimination results are presented and discussed.

2. Material and methods

2.1 Image acquisition

Hyperspectral images of durum wheat have been acquired in an experimental station (INRA, domaine de Melgueil) near Montpellier, south of France, in March 2011. Images were acquired using a device specially developed by Cemagref for in-field short-range hyperspectral imagery. The device consists in a push-broom CCD camera (HySpex VNIR 1600-160, Norsk Elektro Optikk, Norway) fitted on a tractor-mounted motorised rail (figure 1). The camera has a spectral range from 0.4 µm to 1 µm with a spectral resolution of 3.7 nm. The first dimension of the CCD matrix is the spatial dimension (1600 pixels across track) and the second dimension is the spectral dimension (160 bands).

Each image represents about 0.30 m across track by 1.50 m along track seen at 1 m above the canopy, the lens and the view angle being fixed. The spatial resolution across track is 0.2 mm. The spatial resolution along track, depending on the motion speed, has been adjusted consequently.

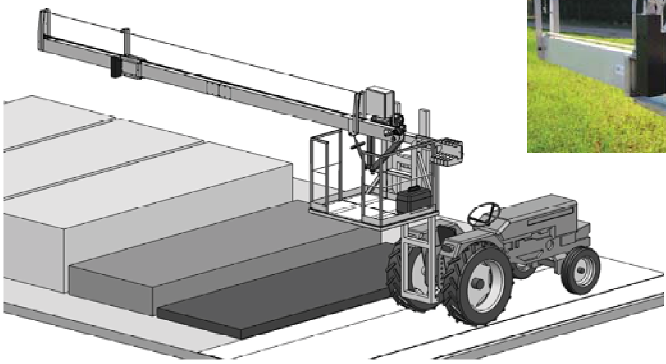


Fig. 1. Cemagref hyperspectral imaging device
Computer Aided Design (CAD) general view and camera detail

Data are digitalised on 12 bits, giving a digital number (DN) between 0 and 2^{12}-1 = 4095. In order to preserve the signal-noise ratio (SNR) while avoiding signal saturation, the CCD sensor integration time has been adjusted for each image so that the average raw signal value for vegetation is around 2000 in the near-infrared domain (where it is maximal). Nevertheless, some pixels are saturated: pixels for which at least one band has a value greater than 4000 have been considered as saturated pixels and their spectra have been automatically set to a null value. They will not be used for further treatments.

In the following, hyperspectral image are shown with false colours, i.e. using 3 bands respectively at 615, 564 and 459 nm as R, G, and B channels.

2.2 Image correction

Luminance correction

Because the CCD sensor has not a uniform spectral sensitivity (it is more sensitive in the visible domain than in the NIR domain), the raw signal must be corrected with data provided by the camera constructor, in order to obtain absolute radiometric data not depending on the instrument. At this stage, other instrumental effects are also taken into account, such as the dark current (which is automatically measured before each image shot with the lens shutter closed), and the relative sensitivity of each CCD pixel. The detailed correction is given by (1)

$$CN[i,j] = \frac{DN[i,j] - BG[i,j]}{RE[i,j].S[j]} \quad (1)$$

where DN[i, j] is the digital number (raw signal), with *i* refering to the first (spatial) dimension of the CCD matrix ($i \in$ [0, 1599]) and *j* refering to the second (spectral) dimension ($j \in$ [0, 159]). BG[i, j], RE[i, j] and S[j] are respectively the dark current, the relative response matrix for each detector element (or pixel) and the camera spectral sensitivity. The resulting float type value CN[i,j] for each line pixel is then a luminance signal. It will be noted $L(x,y,\lambda)$ in the following, where x is the spatial coordinate *i* in the line, y is the spatial coordinate of the line along track, and λ is a given wavelength.

This luminance correction can be made by post-processing, or in real-time during image acquisition. An example of corrected spectrum is given in figure 2.b.

Reflectance correction

In order to be able to compare spectral data collected in different outdoor conditions, we need to have hyperspectral images independent of illumination, i.e. reflectance images. The reflectance of a given material is the ratio of reflected light to incident light. So, we need to know solar lighting at each acquisition time. To this end, Spectralon™ (Labsphere, Inc., New Hampshire, USA.) is generally used because it is a lambertian surface and it reflects 99 % of received signal whatever the wavelength. Therefore, it provides a good approximation of solar incident light in outdoor conditions. However, in our case, we have chosen to use a commercial ceramic plate, which is more robust to damage or dirt due to field experiment conditions. Also, since integration time is optimised for vegetation, a grey ceramic plate was required, in order to avoid saturated ceramic pixels. This plate has been set in the field of view for every image acquisition (see figures 5 and 7).

The bidirectional reflectance distribution function (BRDF) of the ceramic has been measured in laboratory. As for many ordinary materials, it is the summation of a lambertian term and a specular term (shininess), this last one depending on the incident and viewing angles. However, because the specular term is directive enough, it can be totally neglected in our field operating conditions (horizontal plate observed with a zenithal view under non zenithal solar lighting incidence, according to the latitude and season). We can thus consider the ceramic plate as a lambertian material with a known hemispheric reflectance $Rc(\lambda)$.

Finally, for a given luminance image, the average luminance $Lc(\lambda)$ measured on the ceramic plate can be used to compute the horizontal irradiance $E(\lambda)$ on the scene:

$$E(\lambda) = Lc(\lambda) / Rc(\lambda) \qquad (2)$$

This allows to apply the following reflectance correction to every pixel in the image:

$$R(x,y,\lambda) = L(x,y,\lambda) / E(\lambda) = \frac{L(x,y,\lambda).Rc(\lambda)}{Lc(\lambda)} \qquad (3)$$

where (x,y) are the pixel coordinates.

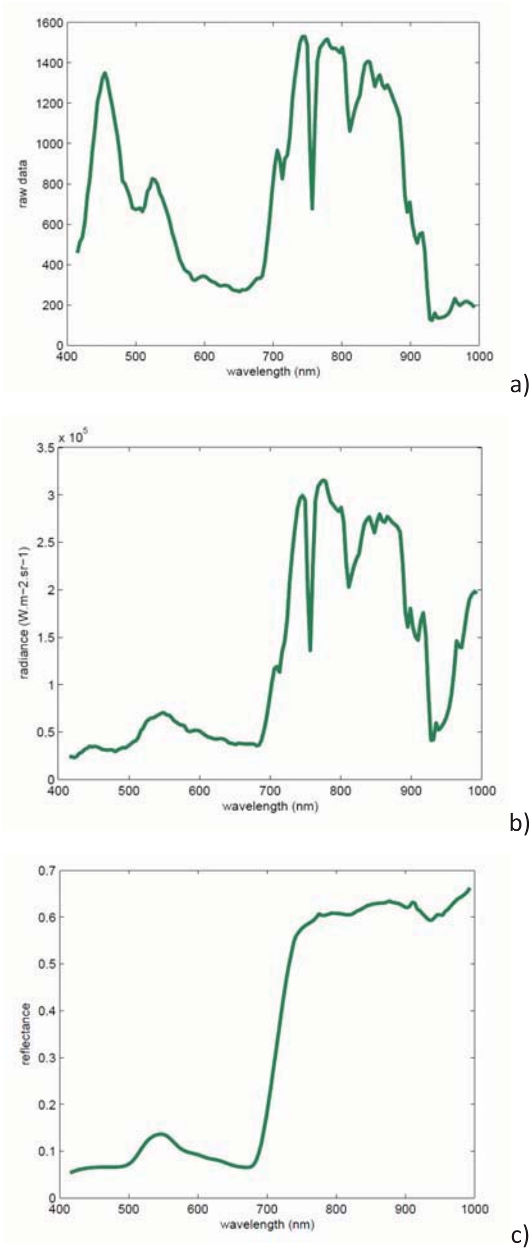

Fig. 2: Example of 12 bits raw spectrum (a), luminance spectrum (b) and reflectance spectrum (c) for a vegetation pixel.

The effect of successive luminance and reflectance corrections on a vegetation pixel are given in figure 2. The reflectance spectrum clearly shows how lighting spectrum specificities are removed, e.g. the absorption peak near 750 nm due to oxygen in the atmosphere.

Leaf-orientation-effect correction

The reflectance correction specified in (3) takes into account the irradiance E(λ) measured by means of an horizontal plate. However, leaf surfaces in the vegetation scene are not horizontal. Therefore, their irradiance can be higher or lower than the ceramic plate's one, according to the cosine of the angle between their surface normal and the lighting incidence (Figure 3.a). This introduces an unknown multiplicative factor *k1* on the pixel spectrum collected in the reflectance image, with respect to the real leaf reflectance.

Moreover, as already mentioned for the ceramic plate, the BRDF of leaves includes a specular term (Bousquet L. et al, 2005). But in this case, due to a random spatial orientation, this specular reflection may be directed toward the image sensor (Figure 3.b). Because the specular light is not spectrally modified by the material, it contributes to the apparent reflectance as an additive term *k2*.

As a summary, the leaf pixel values in the reflectance image do not correspond to the actual leaf lambertian reflectance $Rf(x,y,\lambda)$, but to an apparent reflectance:

$$Rapp(x,y,\lambda) = Rf(x,y,\lambda).k1 + k2 \qquad (4)$$

where *k1* and *k2* are unknown terms.

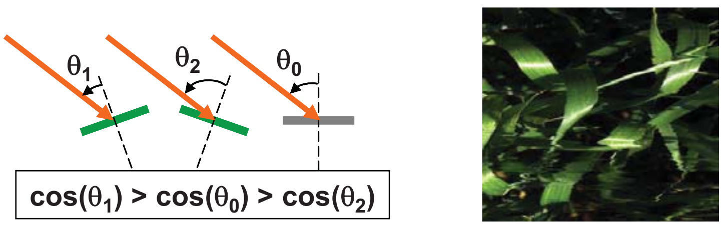

a b

Fig. 3: Leaf **orientation** effects.
a) effect on irradiance level; b) specular reflection

In order to remove these unknown terms, a Standard Normal Variate (SNV) transformation will be systematically applied to every spectrum before any further processing. It consists in centring the spectrum and setting its standard deviation equal to one (Figure 4).

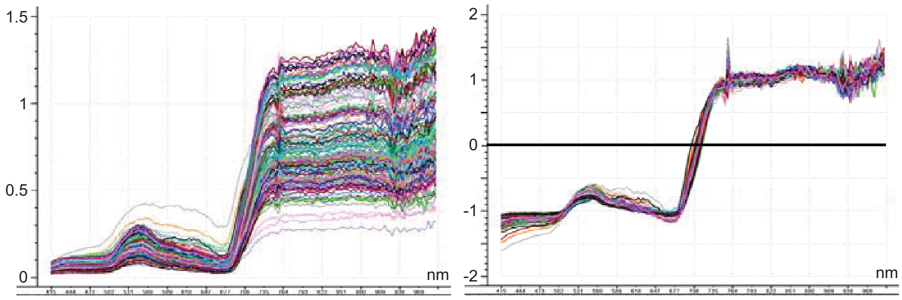

Figure 4: SNV transformation applied to a set of wheat spectra

2.2 Spectral discrimination model

Calibration set

In order to build a discrimination model, we need a calibration set, i.e. a set of spectrum samples for each of the material classes that we want to discriminate. For this purpose, we have selected manually a total of 335 pixels in a reflectance image, according to three classes: durum wheat (157 pixels), dicotyledonous weeds (60 pixels) and soil (118 pixels).

The calibration image is shown in figure 5, as well as the position of the samples. It has been obtained with an integration time of 100 ms per line.

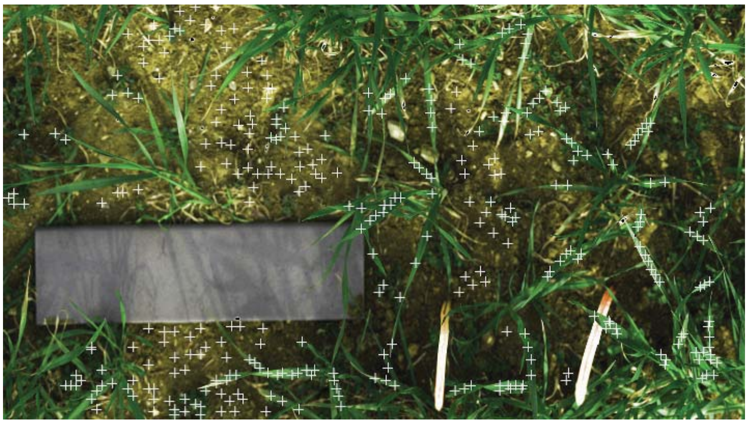

Figure 5: Calibration image and sample positions

PLS-DA discrimination model

Because they contain accurate information about the chemical content of materials, reflectance or transmittance spectra are often used for quantitative evaluation of component concentration, or for material discrimination. However, due to the high dimension of spectral data (hundreds of variables), classical multivariate regression or discrimination tools are not directly usable, and a first step of dimension reduction is generally required. In this context, the Partial-Least-Square regression (PLS) has become a very commonly used tool, thanks to its ability to determinate a pertinent subspace for a given regression problem (unlike other dimension reduction methods like the Principal Component Analysis, the PLS takes into account the covariance of both inputs and outputs to determine the subspace components, called "latent variables" or LV).

The PLS addresses the following linear regression problem: given a set of p calibration spectra $Xp = [S1(\lambda), \ldots, Sp(\lambda)]$ and the corresponding outputs $Yp = [y1, \ldots, yp]$, one wants to define a linear regression model B so that for any input spectrum S, the corresponding output y can be estimated by:

$$y = B.\ S \tag{5}$$

(notice that the standard solution $B = Yp\ .\ Xp^{+}$, where Xp^{+} is the pseudo-inverse of the matrix Xp, is generally undefined due to the high dimensionality of Xp).

The PLS is an iterative method, where a new LV is built at each step. The optimal number of latent variables (LV) is usually determined using an independent test set, or by a leave-one-out procedure (cross-validation).

Though the PLS usually addresses linear regression, it can also be use in discrimination analysis (PLS-DA). In the present case, we have chosen the following PLS-DA procedure:

i) 3 targeted output functions y1, y2, y3 have been defined as the membership level for each of the three classes, with the following values for the calibration set :

y1 = 1 for the wheat class, and 0 otherwise

y2 = 1 for the weed class, and 0 otherwise

y3 = 1 for the soil class, and 0 otherwise

ii) 3 regression models B1, B2, B3 have then been computed by PLS, so that for a given input spectrum S, the membership levels can be estimated by:

$$y1 = B1.S\ ; \qquad y2 = B2.S\ ; \qquad y3 = B3.S$$

iii) the chosen class for the input spectrum S is then the class *i* for which the membership degree y*i* is the higher.

3. Results and discussion

In order to illustrate the classification procedure, the three estimated membership values for all the samples are given in figure 6. As it could be expected, the best membership estimation is obtained for the soil, and requires only two LV (soil could be discriminated easily from vegetation using a few spectral bands).

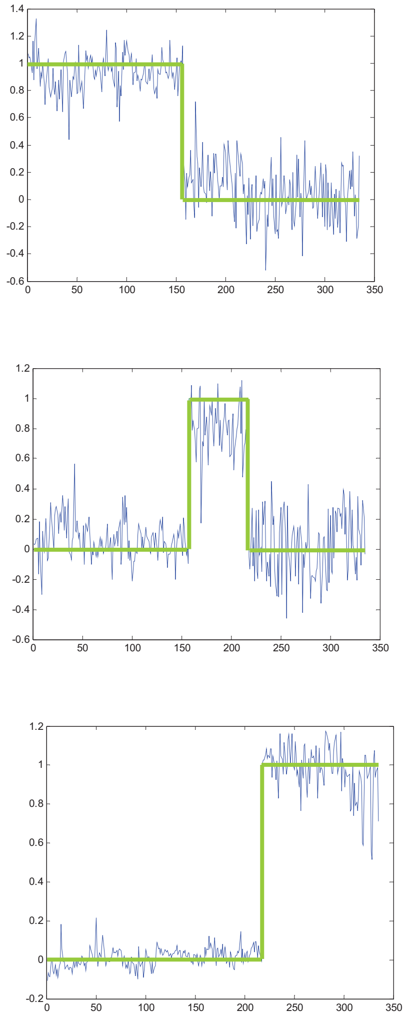

y1 (wheat) (8 LV)

y2 (weed) (8 LV)

y3 (soil) (2 LV)

Figure 6: Membership degree functions estimated by PLS for the 335 samples
on the abscissa: sample number (samples are sorted by class)
in green: targeted binary values

Hyperspectral imagery to discriminate weeds in wheat

As explained above, the classification procedure consists, for a given spectrum, in choosing the class with the highest estimated membership degree. It has first been applied on the calibration set itself, i.e. according to the function values shown in figure 6. The resulting confusion matrix is given in table 1. The classification performances are very good, with a maximal error rate of 1.7 % (dicotyledonous classified as wheat).

	Classified as wheat	Classified as weed	Classified as soil
Wheat	**156 (99.4 %)**	**1 (0.6 %)**	**0**
Weed	**1 (1.7 %)**	**59 (98.3 %)**	**0**
Soil	**0**	**0**	**118 (100 %)**

Table 1: confusion matrix for the whole sample set

Finally, the classification procedure defined above has been applied to a complete test image. This image has been acquired one hour after the calibration image, with an integration time of 50 ms. The original image as well as the corresponding classification results are given in figure 7.

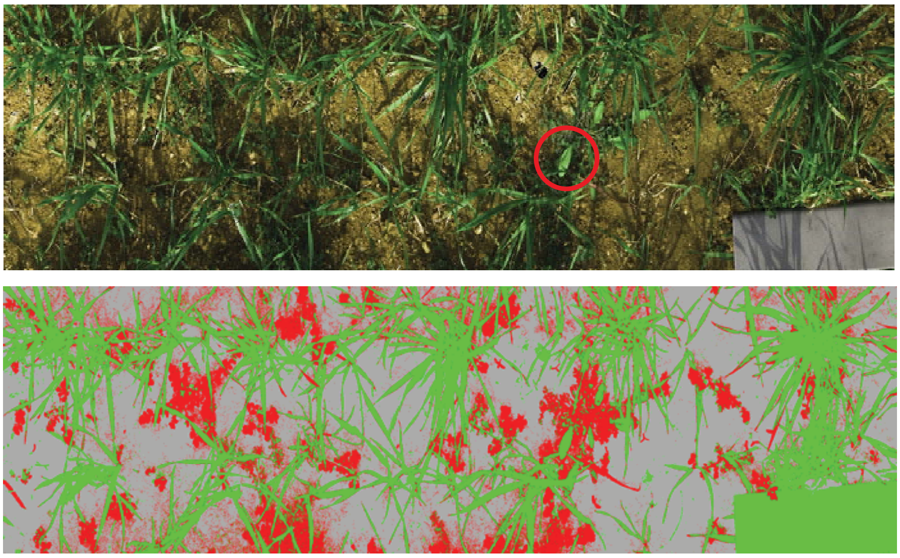

Figure 7: Original test image (up) and classification results (down)
Pixels classified respectively as wheat, weed and soil are colored in green, red and gray. The red circle show a dicotyledonous weed classified as wheat.

This test image confirms the high quality of classification and its robustness with respect to variable local lighting conditions (leaf orientation and shadowed areas). As an exception, a dicotyledonous weed (red circle in figure 7 up) has entirely been classified as wheat: the reason is that this weed specie was not represented in the calibration set, so that its classification is arbitrary (as well as the classification of the ceramic pixels).

4. Conclusion

The results obtained above show the remarkable ability of detailed spectral information to discriminate vegetation species, provided the influence of lighting variability has been overcome using a reference material, and provided efficient chemometric tools such are PLS are involved. However, the classification error in the test image for a weed specie that had not been sampled before, underlines the importance of the calibration set sufficiency. Moreover, the high number of required latent variables (up to eight) indicates that very tiny differences in the spectral shapes are taken into account to achieve an accurate discrimination.

For these reasons, the robustness of such a discrimination model must still be assessed in extended experimental conditions (different days, different parcels, etc.). If the results are satisfactory, the following step will be to evaluate the possibility to reduce the number of required bands, e.g. through a detailed study of the latent variable shapes. It would open the door to an operational device based on multispectral image acquisition.

References

Bousquet L., S. Lachérade, S. Jacquemoud and I. Moya (2005). Leaf BRDF measurement and model for specular and diffuse component differentiation, *Remote Sensing of Environment*, 98(2-3):201-211.

Burks, F.T, S.A. Shearer and F. A. Payne (2000). Classification of weed species using color texture features and discriminant analysis. *Transactions of the ASAE* 43: 441-448.

Chi, T.Y, C.-F. Chien and T.-T. Lin (2003). Leaf shape modeling and analysis using geometric descriptors derived from Bezier curves. *Transactions of the ASAE* 46: 175-185.

Feyaerts, F. and L. van Gool (2001). Multi-spectral vision system for weed detection. *Pattern Recognition Letters* 22(6-7): 667-674.

Gée, C., J. Bossu, G. Jones and F. Truchetet (2008). Crop/weed discrimination in perspective agronomic images. *Computers and Electronics in Agriculture* 60(1): 49-59.

Manh, A.-G., G. Rabatel, L. Assemat, M.-J. Aldon (2001). Weed Leaf Image Segmentation by Deformable Templates. *Journal of Agricultural Engineering Research* 80(N°2): 139-146.

Slaughter, D.C., D.K. Giles and D. Downey (2008). Autonomous robotic weed control systems : A review. *Computers and electronics in agriculture* 61: 63 - 78

Vigneau, N., M. Ecarnot, G. Rabatel, P. Roumet (2011). Potential of field hyperspectral imaging as a non destructive method to assess leaf nitrogen content in Wheat. *Field Crops Research* 122(1): 25-31.

Vrindts, E., J. De Baerdemaeker and H. Ramon (2002). Weed Detection Using Canopy Reflection. *Precision Agriculture* 3(1): 63-80.